*Progress In Electromagnetics Research C, Vol. 114, 83–96, 2021*

# Partial Electrical Equivalent Circuits and Finite Difference Methods Coupling; Application to Eddy Currents Calculation for Conductive and Magnetic Thin Plates

**Saida Djemoui[1], Hicham Allag[1], Mohammed Chebout[2, *], and Houssem R. El-Hana Bouchekara[3]**

**Abstract**—This paper presents a new integro-differential coupling between partial equivalent electrical circuits (PEEC) and finite difference method (FDM) taking into account the magnetization effect. This coupling is intended for thin plates having simultaneously significant conductive and magnetic properties in the presence of exciting coils of complex topologies. These cases exist in eddy current nondestructive testing (ECNDT), eddy current separation, induction or levitation melting devices, and more other applications. The choice of FDM, is in relation with rectangular surfaces generated by numerical meshes leading to mathematical integrations of magnetic and electrical quantities with independent variables, unlike more complicated forms of surfaces generated by finite element method (FEM) or others. Fully successful analytical expressions have been realized and implemented in overall coupling process. The PEEC method is mainly used to calculate the magnetic field applied to the nodes of the plate from different inclined polygonal coils. The results of magnetic field and eddy current distributions on thin plates are presented, and parts of them are compared with those realized by Flux 3D software.

## 1. INTRODUCTION

Accidental or voluntary eddy currents generation in metal objects is a classical well-known phenomenon used in various practical applications. Eddy current nondestructive testing (ECNDT) is one of interesting tools to mainly detect serious cracks in metal plates by measuring impedance changes [1–3]. Eddy current separation is also a relevant method for extricating conducting and magnetic particles from other ores, liquids or grainy manufactured products [4, 5]. In levitation melting, eddy currents are responsible to heat, melt specific objects and already help to repel particles avoiding any direct contact with the container [6, 7]. Another recent technology called electrodynamic sorting uses high-frequency electromagnets to separate conducting metal particles from other of a different physical nature container [8–10]. Electromagnetic damping signifies the creation of a resistive force that causes a conductive object, in which eddy currents flow, to slow down without physically touching it. It is a principle used on rail brakes to help high-speed rail carriages stop at certain points without the need of physical brakes. From the cited applications of eddy currents, a great number of induced regions can be considered as thin. The property of being thin can obey at two different aspects, geometrical and electromagnetic geometrical ones, because the regions have at least one thickness incomparably smaller than the other dimensions, electromagnetically thin, if the thickness is much smaller than the penetration depth of the electromagnetic field [11]. The study and analysis of eddy current distributions in systems containing a thin plate and complex topologies of coils need specific treatments. Several research articles in the field of nondestructive testing (NDT) have addressed the cases of thin materials

*Received 16 May 2021, Accepted 20 July 2021, Scheduled 28 July 2021*

* Corresponding author: Mohammed Chebout (m.chebout@mail.univ-djelfa.dz).

[1] Electrical and Industrial Electronic Laboratory, University of Jijel, L2EI, Algeria. [2] Applied Automation and Industrial Diagnostics Laboratory L2ADI, University of Djelfa, Algeria. [3] Electrical Engineering Department, University of Hafr Al Batin, Saudi Arabia.

whether for the simultaneous measurement of the distance and the thickness of a thin metal plate based on the analytical Deed and Dodd model [12], or the use of the multi-frequency and pulsed eddy current technique for the same reason [13, 14]. Other work has overcome the problems generated by the modeling of thin regions by the finite element method, based on the surface impedance approach [15, 16]. For these types of 3D applications, the direct use of differential approaches, such as finite element method (FEM) or others, is often difficult and may be sometimes inefficient because of meshes generation (generating bi-dimensional elements for thin regions and three-dimensional elements for all other parts of the concerned systems). The partial equivalent electrical circuits (PEEC) method is mainly used for modelling complex electrical interconnections and can be applied to a large range of devices in which the air region is really dominant [17–22]. The developments in classical PEEC method need to be applied for conducting materials by calculating magnetic and electrical interactions (inductances, capacitances for arbitrary oriented parallelepipedic elementary conductors). This technique has the advantage that it is reasonably intuitive to many electrical engineers, and it is easy to integrate the field solver with real circuit elements. Problems can be solved in the time domain or in the frequency domain [23–26]. The major inconvenience of the PEEC resides in its incapability to treat magnetic materials without associating other approaches. In this way, the newest works for coupling PEEC with FEM were realized [27]. For such applications, there exist two types of meshes, the mesh of exciting inductors generated for PEEC method and the mesh of the thin plate by 2D triangular finite elements. In [27–30], the authors implement the magnetization and eddy current effects in thin plates by calculating the result integrals among triangular surfaces of the 2D meshes. These calculations of integrals with dependent geometric variables are not easy to solve, and they are actually issued by numerical ways. In this work, we propose a new coupling between PEEC and FDM in which all the electromagnetic interactions can be expressed analytically and integrated in the total global matrix system to gain more speed and precision when dealing with these three-dimensional electromagnetic problems. Like that, we also benefit from the advantages of the two methods, PEEC and FDM, for which the developments are ceaseless. For FDM, the newest works were developed notably in grids considerations. [31] confirmed that the FDM with hexahedral elements and edge element method have common features. The newest structures of finite-difference schemes were exposed by [32, 33]. [34] proposed the high-order finite-difference schemes for Navier-Stokes 2D equations. By this approach, we also think about 2D materials and thin films caracterization and modelling [35]).

## 2. MATHEMATICAL MODELING

### 2.1. Problem Description

The adopted electromagnetic model for our problem is the same as those approached in [27–30]. The formulation contains the electric potential and magnetization for the thin plate:

$$\begin{cases} \nabla^2 \vec{T} - j\omega\mu\sigma \left(\dfrac{\mu_r}{\mu_r - 1}\right) \vec{M} = 0 \\ \dfrac{\vec{M}(\vec{r})}{\mu_r - 1} + \dfrac{\vec{\nabla}}{4\pi} \displaystyle\int_V \frac{\vec{M}(\vec{r})}{\left|\vec{r} - \vec{r'}\right|^3} \times \left(\vec{r} - \vec{r'}\right) dV' - \frac{1}{4\pi} \int_V \frac{\vec{\nabla} \wedge \left[\vec{T}\left(\vec{r'}\right) \cdot \vec{n}\right] \times \left(\vec{r} - \vec{r'}\right)}{\left|\vec{r} - \vec{r'}\right|^3} dV' = \vec{H_0} \end{cases} \tag{1}$$

In this formulation, eddy currents are assumed to flow tangentially to the plate allow us to consider only a normal component of the electric potential T. The entire problem is composed of a three-dimensional oriented massive coil above a conducting and magnetic thin plate located at the $xOy$ plane of the cartesian coordinate system, Figure 1. The normal applied magnetic field $H_0$ on the plate issued from the massive conductor coils is entirely calculated by PEEC method. From Equation (1), the two integrals will be developed analytically and integrated in FDM process. Applying FDM to the thin plate, we obtain the total matrix system according to Equations (1) and presented as:

$$\begin{bmatrix} [A] & [B] \\ [C] & [D] \end{bmatrix} \cdot \begin{bmatrix} [T] \\ [M] \end{bmatrix} = \begin{bmatrix} [0] \\ [H_0] \end{bmatrix} \tag{2}$$

All the elementary squares matrices ($A$, $B$, $C$, and $D$) have the same size according to the total number of grid nodes.

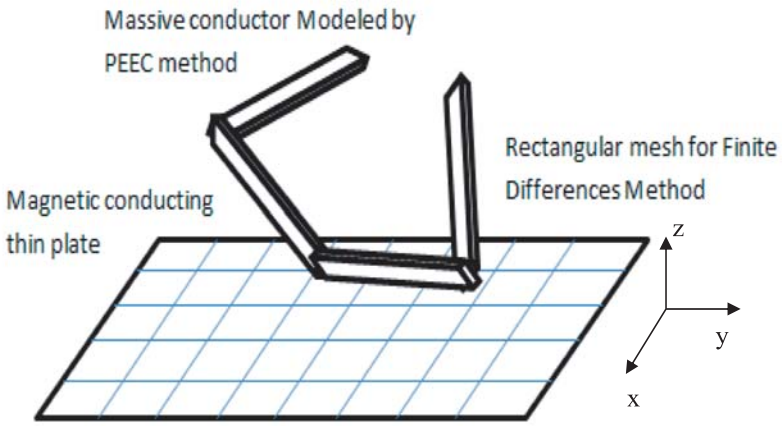


**Figure 1.** Electromagnetic system.

## 2.2. Matrices Developments

*2.2.1. Matrix* $[A]$

Matrix $[A]$ is in relation with Laplacian operator $\nabla^2$. Generally in FDM, the rectangular physical region is composed of a uniform grid. As shown in Figure 2, the ascendant numbering is made respective to $x$ axis (it can also be done for $y$ axis). This regular mesh has a uniform discretisation in the two axes respecting constant steps $\Delta x$ and $\Delta y$. With these considerations, the Laplacian is given:

$$\nabla^2 T = \frac{\partial^2 T}{\partial x^2} + \frac{\partial^2 T}{\partial y^2} = \frac{T(i+1,j) - 2T(i,j) + T(i-1,j)}{\Delta x^2} + \frac{T(i,j+1) - 2T(i,j) + T(i,j-1)}{\Delta y^2} \tag{3}$$

According to the grid shown at Figure 2, we can partially express the Ax and Ay matrices in direct relation with $\dfrac{\partial^2 T}{\partial x^2}$ and $\dfrac{\partial^2 T}{\partial y^2}$, as:

$$A_x = \frac{-1}{\Delta x^2} \begin{bmatrix} \begin{bmatrix} 2 & -1 & \dots & 0 \\ -1 & 2 & -1 & \dots \\ \vdots & 0 & \ddots & 0 \\ 0 & \dots & -1 & 2 \end{bmatrix} & \begin{bmatrix} 0 & 0 & \dots & 0 \\ 0 & 0 & \dots & 0 \\ \vdots & 0 & \ddots & 0 \\ 0 & 0 & \dots & 0 \end{bmatrix} & \cdots & \begin{bmatrix} 0 & 0 & \dots & 0 \\ 0 & 0 & \dots & 0 \\ \vdots & 0 & \ddots & 0 \\ 0 & 0 & \dots & 0 \end{bmatrix} \\ \begin{bmatrix} 0 & 0 & \dots & 0 \\ 0 & 0 & \dots & 0 \\ \vdots & 0 & \ddots & 0 \\ 0 & 0 & \dots & 0 \end{bmatrix} & \begin{bmatrix} 2 & -1 & \dots & 0 \\ -1 & 2 & -1 & \dots \\ \vdots & 0 & \ddots & 0 \\ 0 & \dots & -1 & 2 \end{bmatrix} & \cdots & \begin{bmatrix} 0 & 0 & \dots & 0 \\ 0 & 0 & \dots & 0 \\ \vdots & 0 & \ddots & 0 \\ 0 & 0 & \dots & 0 \end{bmatrix} \\ \vdots & \vdots & \ddots & \vdots \\ \begin{bmatrix} 0 & 0 & \dots & 0 \\ 0 & 0 & \dots & 0 \\ \vdots & 0 & \ddots & 0 \\ 0 & 0 & \dots & 0 \end{bmatrix} & \begin{bmatrix} 0 & 0 & \dots & 0 \\ 0 & 0 & \dots & 0 \\ \vdots & 0 & \ddots & 0 \\ 0 & 0 & \dots & 0 \end{bmatrix} & \cdots & \begin{bmatrix} 2 & -1 & \dots & 0 \\ -1 & 2 & -1 & \dots \\ \vdots & 0 & \ddots & 0 \\ 0 & \dots & -1 & 2 \end{bmatrix} \end{bmatrix} \tag{4}$$

A little difference is obtained for $Ay$. The two adjacent values will be situated in different

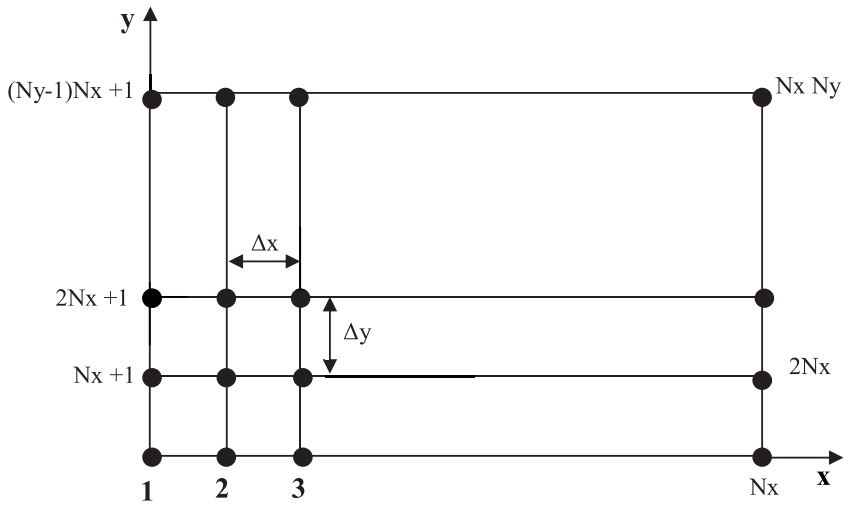


**Figure 2.** Finite difference mesh adopted for thin plate.

submatrices:

$$A_y = \frac{-1}{\Delta y^2}\begin{bmatrix} \begin{bmatrix} 2 & 0 & \dots & 0 \\ 0 & 2 & \dots & 0 \\ \vdots & 0 & \ddots & 0 \\ 0 & 0 & \dots & 2 \end{bmatrix} & \begin{bmatrix} -1 & 0 & \dots & 0 \\ 0 & -1 & \dots & 0 \\ \vdots & 0 & \ddots & 0 \\ 0 & 0 & \dots & -1 \end{bmatrix} & \cdots & \begin{bmatrix} 0 & 0 & \dots & 0 \\ 0 & 0 & \dots & 0 \\ \vdots & 0 & \ddots & 0 \\ 0 & 0 & \dots & 0 \end{bmatrix} \\ \begin{bmatrix} -1 & 0 & \dots & 0 \\ 0 & -1 & \dots & 0 \\ \vdots & 0 & \ddots & 0 \\ 0 & 0 & \dots & -1 \end{bmatrix} & \begin{bmatrix} 2 & 0 & \dots & 0 \\ 0 & 2 & \dots & 0 \\ \vdots & 0 & \ddots & 0 \\ 0 & 0 & \dots & 2 \end{bmatrix} & \cdots & \begin{bmatrix} 0 & 0 & \dots & 0 \\ 0 & 0 & \dots & 0 \\ \vdots & 0 & \ddots & 0 \\ 0 & 0 & \dots & 0 \end{bmatrix} \\ \vdots & \vdots & \ddots & \vdots \\ \begin{bmatrix} 0 & 0 & \dots & 0 \\ 0 & 0 & \dots & 0 \\ \vdots & 0 & \ddots & 0 \\ 0 & 0 & \dots & 0 \end{bmatrix} & \begin{bmatrix} 0 & 0 & \dots & 0 \\ 0 & 0 & \dots & 0 \\ \vdots & 0 & \ddots & 0 \\ 0 & 0 & \dots & 0 \end{bmatrix} & \cdots & \begin{bmatrix} 2 & 0 & \dots & 0 \\ 0 & 2 & \dots & 0 \\ \vdots & 0 & \ddots & 0 \\ 0 & 0 & \dots & 2 \end{bmatrix} \end{bmatrix} \tag{5}$$

Finally, the full matrix $[A]$ is reached by adding $Ax$ and $Ay$ (Equation (3)).

*2.2.2. Matrix* $[B]$

$[B]$ is a diagonal matrix with the same dimension of $A$, and it is expressed according to Equation (1):

$$[B] = \frac{j\omega\mu\sigma\mu_r}{\mu_r - 1}\begin{bmatrix} \begin{bmatrix} 1 & 0 & \dots & 0 \\ 0 & 1 & \dots & 0 \\ \vdots & 0 & \ddots & 0 \\ 0 & 0 & \dots & 1 \end{bmatrix} & \begin{bmatrix} 0 & 0 & \dots & 0 \\ 0 & 0 & \dots & 0 \\ \vdots & 0 & \ddots & 0 \\ 0 & 0 & \dots & 0 \end{bmatrix} & \cdots & \begin{bmatrix} 0 & 0 & \dots & 0 \\ 0 & 0 & \dots & 0 \\ \vdots & 0 & \ddots & 0 \\ 0 & 0 & \dots & 0 \end{bmatrix} \\ \begin{bmatrix} 0 & 0 & \dots & 0 \\ 0 & 0 & \dots & 0 \\ \vdots & 0 & \ddots & 0 \\ 0 & 0 & \dots & 0 \end{bmatrix} & \begin{bmatrix} 1 & 0 & \dots & 0 \\ 0 & 1 & \dots & 0 \\ \vdots & 0 & \ddots & 0 \\ 0 & 0 & \dots & 1 \end{bmatrix} & \cdots & \begin{bmatrix} 0 & 0 & \dots & 0 \\ 0 & 0 & \dots & 0 \\ \vdots & 0 & \ddots & 0 \\ 0 & 0 & \dots & 0 \end{bmatrix} \\ \vdots & \ddots & & \vdots \\ \begin{bmatrix} 0 & 0 & \dots & 0 \\ 0 & 0 & \dots & 0 \\ \vdots & 0 & \ddots & 0 \\ 0 & 0 & \dots & 0 \end{bmatrix} & \begin{bmatrix} 0 & 0 & \dots & 0 \\ 0 & 0 & \dots & 0 \\ \vdots & 0 & \ddots & 0 \\ 0 & 0 & \dots & 0 \end{bmatrix} & \cdots & \begin{bmatrix} 1 & 0 & \dots & 0 \\ 0 & 1 & \dots & 0 \\ \vdots & 0 & \ddots & 0 \\ 0 & 0 & \dots & 1 \end{bmatrix} \end{bmatrix} = \frac{j\omega\mu\sigma\mu_r}{(\mu_r - 1)}[Id] \tag{6}$$

$[Id]$ is the identity matrix of the same size as $[B]$.

*2.2.3. Matrix [C]*

All the original developments are made for constructing $[C]$ and $[D]$ matrices. The hardest work resides in resolving multiple integrals and exploiting the obtaining analytical expressions for building the cited matrices. For the matrix $[C]$ corresponding to the present expression (see Equation (1)), we have the term:

$$\frac{1}{4\pi}\int\limits_{V}\frac{\vec{\nabla}\wedge\left[\vec{T}\left(\vec{r'}\right)\cdot\vec{n}\right]\times\left(\vec{r}-\vec{r'}\right)}{\left|\vec{r}-\vec{r'}\right|^{3}}dV'=\frac{e}{4\pi}\int\limits_{x'}\int\limits_{y'}\frac{\vec{\nabla}\wedge\left[\vec{T}\left(\vec{r'}\right)\cdot\vec{n}\right]\times\left(\vec{r}-\vec{r'}\right)}{\left|\vec{r}-\vec{r'}\right|^{3}}\mathrm{d}x'\mathrm{d}y' \tag{7}$$

First, we develop the expressions inside the volumic integral. Consequently, we obtain:

$$\vec{\nabla}\wedge\vec{T}\left(\vec{r'}\right)=\left(\frac{\partial T}{\partial y}\vec{i}-\frac{\partial T}{\partial x}\vec{j}\right) \tag{8}$$

$$\vec{\nabla}\wedge\vec{T}\left(\vec{r'}\right)\times\left(\vec{r}-\vec{r'}\right)=\left(\frac{\partial T}{\partial y}\left(y-y'\right)+-\frac{\partial T}{\partial x}\left(x-x'\right)\right)\vec{k} \tag{9}$$

The last expression to be integrated becomes:

$$\frac{e}{4\pi}\int\limits_{\frac{-\Delta x'}{2}}^{\frac{\Delta x'}{2}}\int\limits_{\frac{-\Delta y'}{2}}^{\frac{\Delta y'}{2}}\left(\frac{\frac{\partial T}{\partial y}\left(y-y'\right)}{\sqrt{\left(x-x'\right)^{2}+\left(y-y'\right)^{2}}^{3}}+\frac{\frac{\partial T}{\partial x}\left(x-x'\right)}{\sqrt{\left(x-x'\right)^{2}+\left(y-y'\right)^{2}}^{3}}\right)dx'dy' \tag{10}$$

After all integrations, we obtain a pure analytical expression:

$$\begin{aligned}&\frac{3eT}{2\pi}\left[\frac{\sqrt{\left(x-x'\right)^{2}+\left(y-y'\right)^{2}}}{\left(x-x'\right)\left(y-y'\right)}\right]_{\frac{-\Delta x'}{2}}^{\frac{\Delta x'}{2}}\Bigg|_{\frac{-\Delta y'}{2}}^{\frac{\Delta y'}{2}}\\&=T\frac{3e}{2\pi}\sum_{p=0}^{1}\sum_{q=0}^{1}(-1)^{p+q}\left[\frac{\sqrt{\left(x-(-1)^{p}\cdot\frac{\Delta x'}{2}\right)^{2}+\left(y-(-1)^{q}\cdot\frac{\Delta y'}{2}\right)^{2}}}{\left(x-(-1)^{p}\cdot\frac{\Delta x'}{2}\right)\cdot\left(y-(-1)^{q}\cdot\frac{\Delta y'}{2}\right)}\right]\end{aligned} \tag{11}$$

In this last expression, we denote the presence of the variables $(x, y)$ and $(x', y')$. The $x$ and $y$ present the calculation point coordinates in the thin plate, and $x'$ and $y'$ are the elementary element coordinates from the thin plate interacting with all elements generated by the regular grid according to FDM consideration Figure 3 and Figure 4.

To avoid possible singularities known in integral approaches and to have same matrices sizes, we choose the calculation points identical to real nodes, but for integrals calculation, the corresponding elements are generated by another fictive grid (see discontinuous lines configuration in Figure 4. For simplifying the matrix forme, we can write the matrix $[C]$ as:

$$[C_{ij}]=\frac{3e}{2\pi}\sum_{p=0}^{1}\sum_{q=0}^{1}(-1)^{p+q}\left[\frac{\sqrt{\left(\left(x_i-x_j+(-1)^{p}\cdot\frac{\Delta x'}{2}\right)\right)^{2}+\left(\left(y_i-y_j+(-1)^{q}\cdot\frac{\Delta y'}{2}\right)\right)^{2}}}{\left(\left(x_i-x_j+(-1)^{p}\cdot\frac{\Delta x'}{2}\right)\right)\cdot\left(\left(y_i-y_j+(-1)^{q}\cdot\frac{\Delta y'}{2}\right)\right)}\right] \tag{12}$$

The $i$ and $j$ indices correspond respectively to the observation point and the center of the rectangular element.

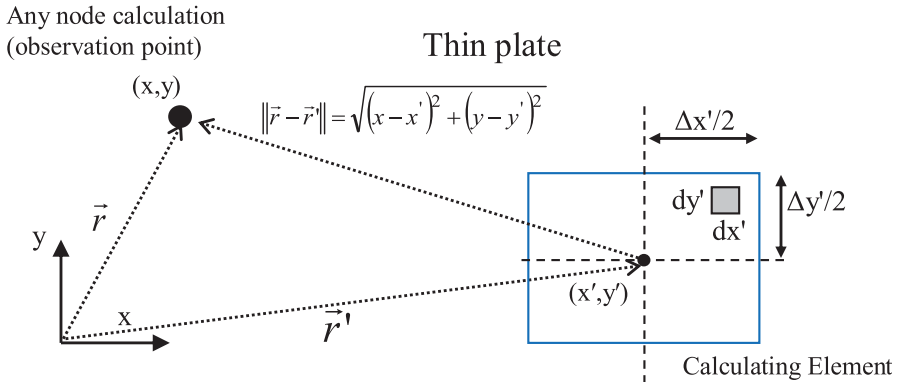


**Figure 3.** Calculation principle on the thin plate.

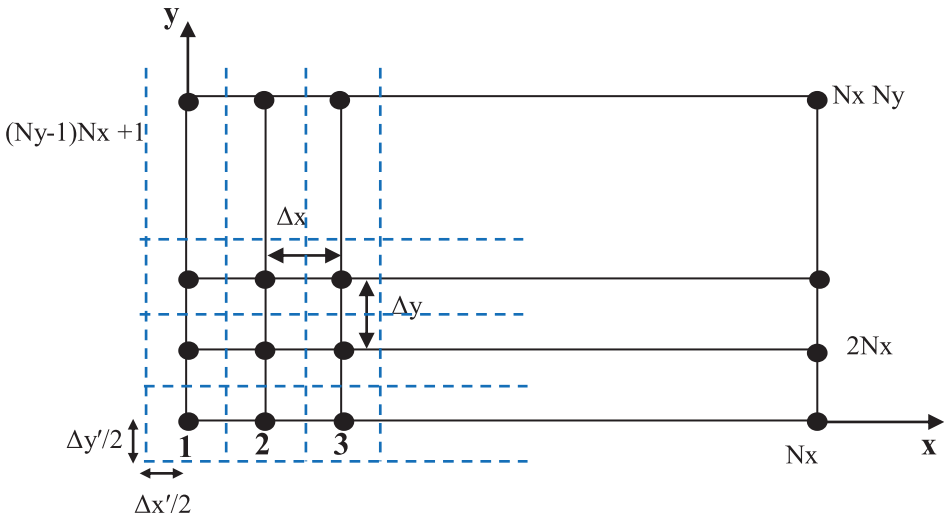


**Figure 4.** Grids and nodes presentation.

### *2.2.4. Matrix* $[D]$

The main influencing term in matrix $[D]$ always has an integral form (Equation (1)). It can be expressed by another manner as:

$$\frac{\vec{\nabla}}{4\pi}\int_V \frac{\vec{M}(\vec{r})}{\left|\vec{r}-\vec{r'}\right|^3}\times\left(\vec{r}-\vec{r'}\right)dV' = \frac{1}{4\pi}\int_V\left[\frac{-\vec{M}\left(\vec{r'}\right)}{\left|\vec{r}-\vec{r'}\right|^3}+3\frac{\vec{M}\left(\vec{r'}\right)\times\left(\vec{r}-\vec{r'}\right)}{\left|\vec{r}-\vec{r'}\right|^5}\left(\vec{r}-\vec{r'}\right)\right]dV' \tag{13}$$

The magnetization $M$ is assumed to be co-linear with the applied magnetic field and normal to the surface of the thin plate [1, 2]. In this case, the second term of Equation (13) will be neglected (scalar product). From the last expression, the first term will only be considered:

$$\frac{\vec{\nabla}}{4\pi}\int_V \frac{\vec{M}\left(\vec{r'}\right)\cdot\left(\vec{r}-\vec{r'}\right)}{\left|\vec{r}-\vec{r'}\right|^3}dV' = \frac{-e}{2\pi}M\left[\frac{\sqrt{(x-x')^2+(y-y')^2}}{(x-x')(y-y')}\right]_{\frac{-\Delta x'}{2}}^{\frac{\Delta x'}{2}}\Bigg|_{\frac{-\Delta y'}{2}}^{\frac{\Delta y'}{2}} \tag{14}$$

We take the same considerations as in developing $[C]$ matrix, and respecting Equations (1) and (2), we obtain:

$$[D] = \frac{1}{\mu_r - 1}([Id] + [D_{ij}]) \tag{15}$$

$$[D_{ij}] = \frac{e}{2\pi}\sum_{p=0}^{1}\sum_{q=0}^{1}(-1)^{p+q}\left[\frac{\sqrt{\left(\left(x_i - x_j + (-1)^p \cdot \frac{\Delta x'}{2}\right)\right)^2 + \left(\left(y_i - y_j + (-1)^q \cdot \frac{\Delta y'}{2}\right)\right)^2}}{\left(\left(x_i - x_j + (-1)^p \cdot \frac{\Delta x'}{2}\right)\right)\cdot\left(\left(y_i - y_j + (-1)^q \cdot \frac{\Delta y'}{2}\right)\right)}\right] \tag{16}$$

*2.2.5. Calculation of [H0] Vector by PEEC Method*

Because of complex topologies of massive conductors for exciting coils near the thin plate, we develop a three-dimensional procedure and compute the magnetic field in the thin plate according to the regular mesh imposed by the FDM considerations. Our goal is to always consider the plate at the $xOy$ plane and the inclined configuration for the coil. Initially, we can realize the calculation procedure for an arbitrary oriented conductor element of the coil, indicated by $(n)$ Figure 5. The basis model consists of a calculation of magnetic field produced by an elementary parallelepipedic conductor $(n)$ carrying constant current $I_n$ in $X_n$ direction and placed in a center of the local axis $OnXnYnZn$ also defined in global reference $Oxyz$, as shown in Figure 5. This model was adopted by us for only one angle of inclination [36, 37]. In this case, two angles will be considered ($\Theta$ and $\Psi$ for Euler transformations consideration). The only component $A_{X_n}$ is defined in its local reference. At any point M according to $O_nX_nY_nZ_n$, the magnetic vector potential component $A_{X_n}$ is given as:

$$A_{x_n} = \frac{\mu_0}{4\pi}\int_{-cn}^{cn}\int_{-bn}^{bn}\int_{-an}^{an}\left(\frac{J_x}{\left|\vec{R}\right|}dX_n dY_n dZ_n\right) \tag{17}$$

with

$$\left|\vec{R}\right| = \sqrt{\left(X_{c_n} - X_n\right)^2 + \left(Y_{c_n} - Y_n\right)^2 + \left(Z_{c_n} - Z_n\right)^2} \tag{18}$$

We can obtain the magnetic fields by:

$$\vec{H} = \frac{\vec{\nabla} \times \vec{A}}{\mu_0} \tag{19}$$

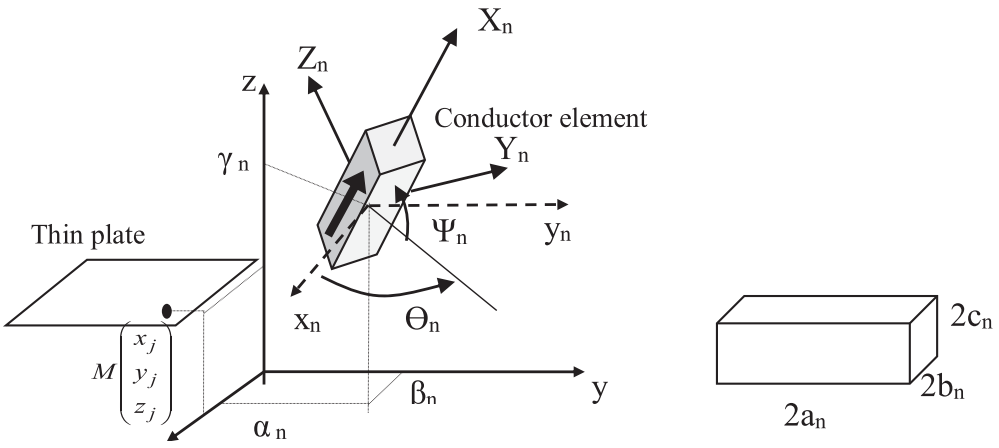


**Figure 5.** Arbitrary oriented coil conductor element.

After all integrations of Eq. (17) and applying the rotational expression (19), the solution of magnetic field components is given by intermediary variables, $U_n$, $V_n$, and $W_n$.

$$H_{Yn} = \frac{J_x}{4\pi}\sum_{i=0}^{1}\sum_{j=0}^{1}\sum_{k=0}^{1}(-1)^{i+j+k}\left(U_n\ln(r_n-V_n)+V_n\ln(r_n-U_n)+W_n\tan^{-1}\left(\frac{U_nV_n}{W_nr_n}\right)\right) \tag{20}$$

$$H_{Zn} = \frac{J_x}{4\pi}\sum_{i=0}^{1}\sum_{j=0}^{1}\sum_{k=0}^{1}(-1)^{i+j+k}\left(-U_n\ln(r_n-W_n)-W_n\ln(r_n-U_n)-V_n\tan^{-1}\left(\frac{U_nW_n}{V_nr_n}\right)\right) \tag{21}$$

with the intermediary variables, $U_n$, $V_n$, and $W_n$, respectively:

$$\begin{cases} U_n = X_{c_n} - (-1)^i a_n \\ V_n = Y_{c_n} - (-1)^j b_n \\ W_n = Z_{c_n} - (-1)^k c_n \\ r_n = \sqrt{U_n^2+V_n^2+W_n^2} \end{cases} \tag{22}$$

It is interesting to define the magnetic field at the same point $M(x,y,z)$ defined in the absolute reference $Oxyz$ and according to direct rotation using Euler transformations matrices (around $z$ axis and $y$ axis)

$$\begin{bmatrix} X_{c_n} \\ Y_{c_n} \\ Z_{c_n} \end{bmatrix} = \begin{bmatrix} \cos\theta_n & \sin\theta_n & 0 \\ -\sin\theta_n & \cos\theta_n & 0 \\ 0 & 0 & 1 \end{bmatrix}\begin{bmatrix} \cos\psi_n & 0 & -\sin\psi_n \\ 0 & 1 & 0 \\ \sin\psi_n & 0 & \cos\psi_n \end{bmatrix}\begin{bmatrix} x_j-\alpha_n \\ y_j-\beta_n \\ z_j-\gamma_n \end{bmatrix} = [T_n]\begin{bmatrix} x_j-\alpha_n \\ y_j-\beta_n \\ z_j-\gamma_n \end{bmatrix} \tag{23}$$

$$\begin{aligned}[T_n] &= \begin{bmatrix} \cos\theta_n & \sin\theta_n & 0 \\ -\sin\theta_n & \cos\theta_n & 0 \\ 0 & 0 & 1 \end{bmatrix}\begin{bmatrix} \cos\psi_n & 0 & -\sin\psi_n \\ 0 & 1 & 0 \\ \sin\psi_n & 0 & \cos\psi_n \end{bmatrix} \\ &= \begin{bmatrix} \cos\theta_n\cos\psi_n & \sin\theta_n & -\cos\theta_n\sin\psi_n \\ -\sin\theta_n\cos\psi_n & \cos\theta_n & \sin\theta_n\sin\psi_n \\ \sin\psi_n & 0 & \cos\psi_n \end{bmatrix}\end{aligned} \tag{24}$$

$$\begin{cases} U_n = (x_j-\alpha_n)\cos\theta_n\cos\psi_n+(y_j-\beta_n)\sin\theta_n-(z_j-\gamma_n)\cos\theta_n\sin\psi_n-(-1)^i a_n \\ V_n = -(x_j-\alpha_n)\sin\theta_n\cos\psi_n+(y_j-\beta_n)\cos\theta_n+(z_j-\gamma_n)\sin\theta_n\sin\psi_n-(-1)^j b_n \\ W_n = (x_j-\alpha_n)\sin\psi_n+(z_j-\gamma_n)\cos\psi_n-(-1)^k c_n \end{cases} \tag{25}$$

From the vector potential component in the inclined local referential, we can now calculate the magnetic field in the general basis referential $Oxyz$ by the inverse transformation matrix.

$$\begin{bmatrix} H_{x_n} \\ H_{y_n} \\ H_{z_n} \end{bmatrix} = [T_n]^{-1}\begin{bmatrix} 0 \\ H_{Y_n} \\ H_{Z_n} \end{bmatrix} \tag{26}$$

$$[T_n]^{-1} = \begin{bmatrix} \cos\theta_n\cos\psi_n & -\sin\theta_n\cos\psi_n & \sin\psi_n \\ \sin\theta_n & \cos\theta_n & 0 \\ -\cos\theta_n\sin\psi_n & \sin\theta_n\sin\psi_n & \cos\psi_n \end{bmatrix} \tag{27}$$

$$H_{xn} = -H_{Yn}\sin\theta_n\cos\psi_n + H_{Zn}\sin\psi_n \tag{28}$$

$$H_{yn} = H_{Yn}\cos\theta_n \tag{29}$$

$$H_{zn} = H_{Yn}\sin\theta_n\sin\psi_n + H_{Zn}\cos\psi_n \tag{30}$$

To validate our developments, we apply this basic principle to calculate the magnetic field around different coils. For all cuboidal elements (Nseg) of the closed coil, each segment is defined simultaneously by its inclined angle and proper dimensions. The total magnetic vector potential becomes:

$$H_x = \sum_{n=1}^{Nseg} H_{xn} \qquad H_x = \sum_{n=1}^{Nseg} H_{xn} \qquad H_z = \sum_{n=1}^{Nseg} H_{zn} \tag{31}$$

According to the thin plate placed in $Oxy$ plane, only the $H_z$ component will be considered. The vector $H_{0j}$ is defined according to the node coordinates ($x_j$, $y_j$, and $z_i = cst$)

$$H_{0j} = H_{zj} \tag{32}$$

### 2.3. Calculation Summary

The total calculation steps for determining eddy currents and magnetization can be respectively summarized as:

**Partial equivalent electrical circuits (PEEC) Method**

1. Number and dimensions of all $(n)$ linear massive conductors $(N_{seg}, a_n, b_n, c_n)$.
2. Centers coordinates of parallelipipedic conductors $(\alpha_n, \beta_n, \gamma_n)$.
3. Inclined angles ($\theta_n$ and $\psi_n$).
4. Rectangular grid coordinates of thin plate in $Oxy$ plane ($x_j, y_j$ and $z_j = cst$).
5. Calculation of $(X_{Cn}, Y_{Cn}$ and $Z_{Cn})$ from Equation (23).
6. Calculation of $(U_n, V_n, W_n$ and $r_n)$ from Equation (22).
7. Calculation of **local** elementary magnetic field components in Equations (20) and (21).
8. Calculation of **global** magnetic field components in thin plate Equations (28) to (30).
9. Calculation of **global** field components from all coil in thin plate Equation (31).
10. From results, we calculate $H_0$ the normal field component on thin plate Equation (32).

**Finite difference method-FDM**

11. Generating the matrices $[A]$, $[B]$, $[C]$ and $[D]$ from respectively Equations (4), (5), (6), (12) and (16).
12. Resolving the global matrix system Equation (2).

### 2.4. Applications

*2.4.1. Calculation of Magnetic Field on Thin Plate from Polygonal Arbitrary Oriented Coils*

To compose aimed polygonal shapes, we demonstrate the manner to consider several topologies of massive coils by generating multiple parallelipepedic conductors, to compose the aimed polygonal shapes. Figure 6 shows rectangular and hexagonal coils. For hexagonal form, we have demonstrated the numbering of conductor segments to reach the total number defined by $Nseg = 6$. Each segment is inclined by $\theta_n$ and $\Psi_n$ versus the global $x$ axis (element 2 was chosen for demonstration).

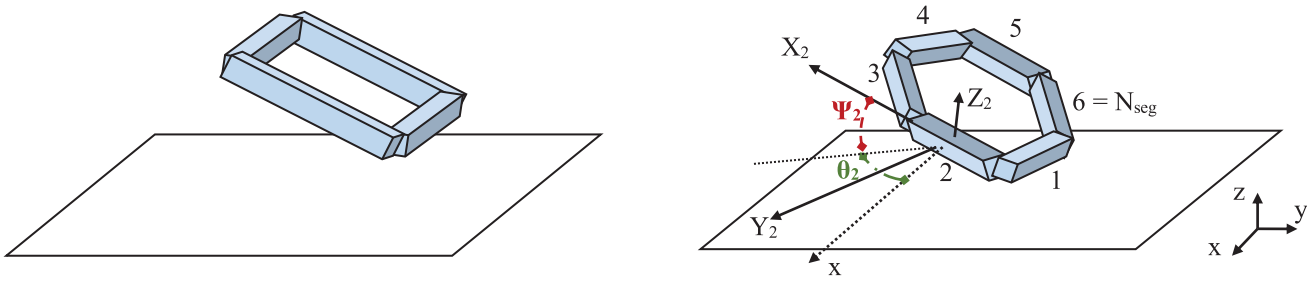


**Figure 6.** Arbitrary oriented polygonal coils.

We generate regular polygons by respecting the chosen circle circumference. The $\theta_n$ angles are increased by a constant angle equivalent to $(360/Nseg)$ in degree. The $\Psi_n$ angles are generally constant and equal for all massive conductor's bloc, and they are responsible of coil tilt. It is also possible to generate more complex and arbitrary configurations by imposing corner points, which respectively link two adjacent parallelepedic conductors. The conducting ferromagnetic plate has a conductivity $\sigma = 9.6\,\mathrm{MS/m}$ and relative permeability $\mu_r = 50$ [1]. The thickness is $e = 1.5\,\mathrm{mm}$, and the dimension is $200 \times 200\,\mathrm{mm}$. A square coil of dimension $100 \times 100\,\mathrm{mm}$ is placed above this plate, inclined by 30° and supplied with a current of 1 A and cross section of the coil ($2a \times 2b = 6 \times 6\,\mathrm{mm}$) Figure 7(a).

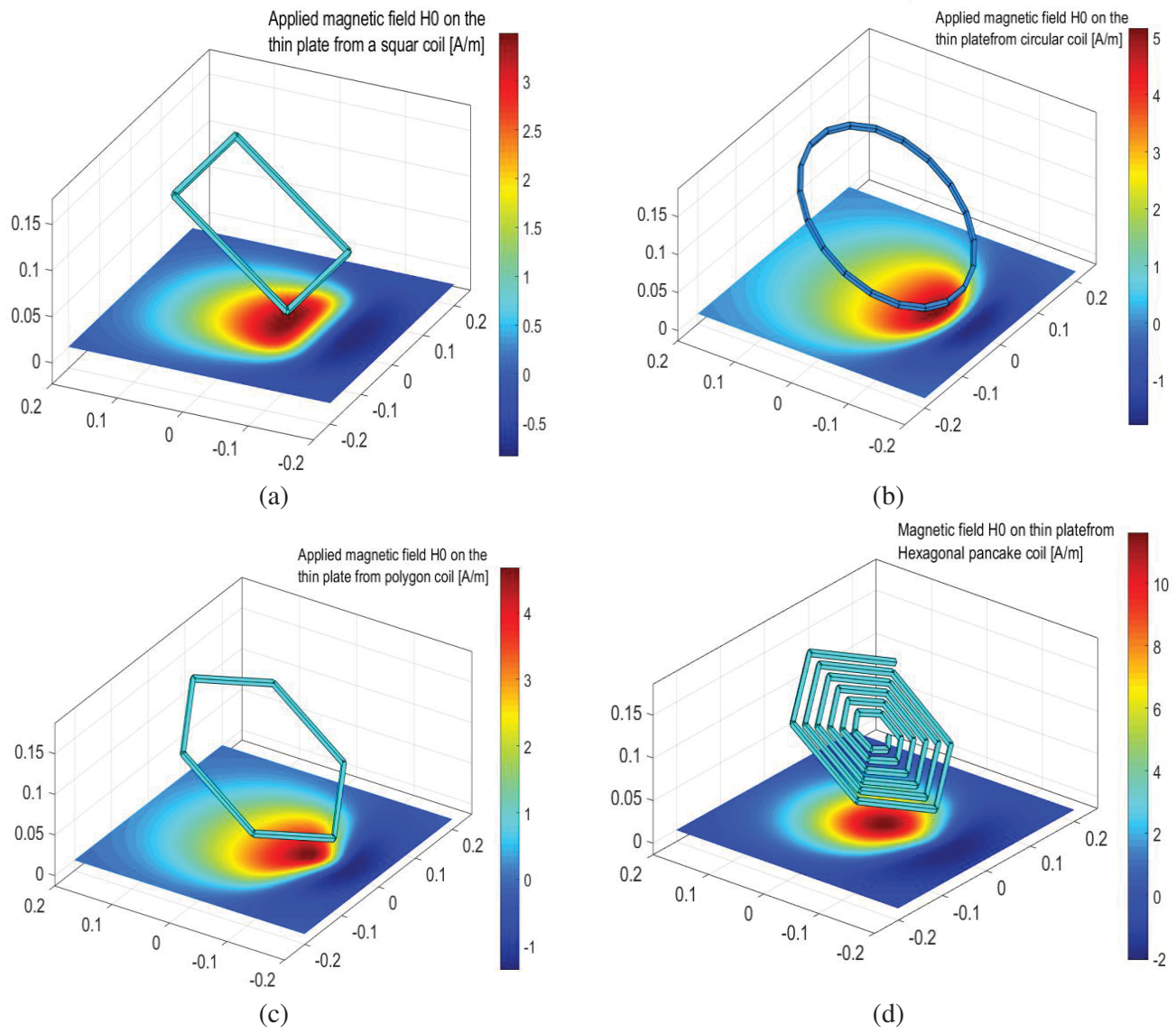


**Figure 7.** Calculated magnetic field from different coil configurations.

With the same diametral distance and increasing the number of segments to $Nseg = 20$, we can obtain a circular loop configuration and its magnetic field generated on the same plate Figure 7(b). A hexagonal coil is obtained for $Nseg = 6$ Figure 7(c), and its generated magnetic field intensity is situated between the square and circular loops because of the differences in elementary conductors number and the enclosed surface. Figure 7(d) demonstrates a magnetic field concentration possibility from an hexagonal pancake coil of 6 turns starting from an outer diameter. All the results of Figure 7

were obtained by programming our approach in Matlab software. The FDM grid was imposed in $XY$ plane, and the coils were shaped by patch elements. By this way, we can also build more complex coils configurations by implementing arbitrary shapes, hence the strength of this PEEC model is associated with Euler's geometric transformations.

### *2.4.2. Calculation of Eddy Currents on Thin Plate*

After calculating eddy current distribution on a thin plate by PEEC/FD model, we now validate, in Figure 8 and Figure 9, the same prototype under the equivalent physical considerations using Flux3D finite element software. The curly shape of the currents for 50 Hz power supply is observed for the two approaches. Globally, the two models present similar eddy current densities in which we can observe the highest values in the closer zone between the coil and the plate. For more precise presentation results, we choose one line segment on the plate parallel to $y$-axis, defined by the two points $(0, -0.15)$ $(0, 0.15)$ Figure 10. For this line path, we display the calculated eddy currents by the two methods.

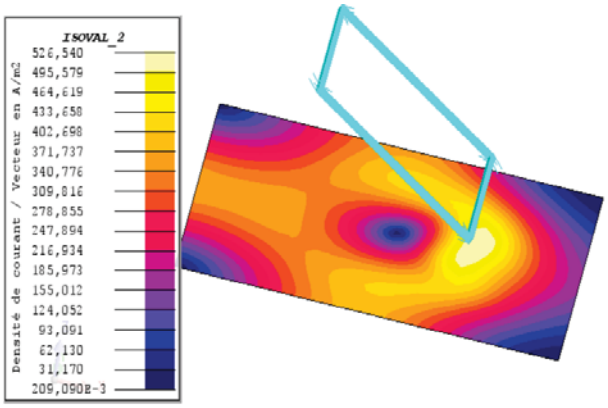


**Figure 8.** Eddy current calculation by FEM Flux3D.

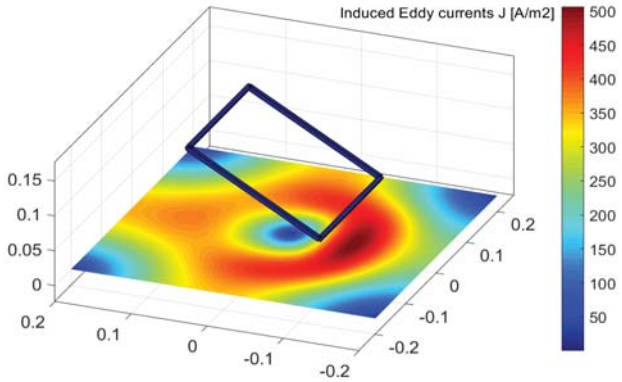


**Figure 9.** Eddy current calculation by PEEC/FD.

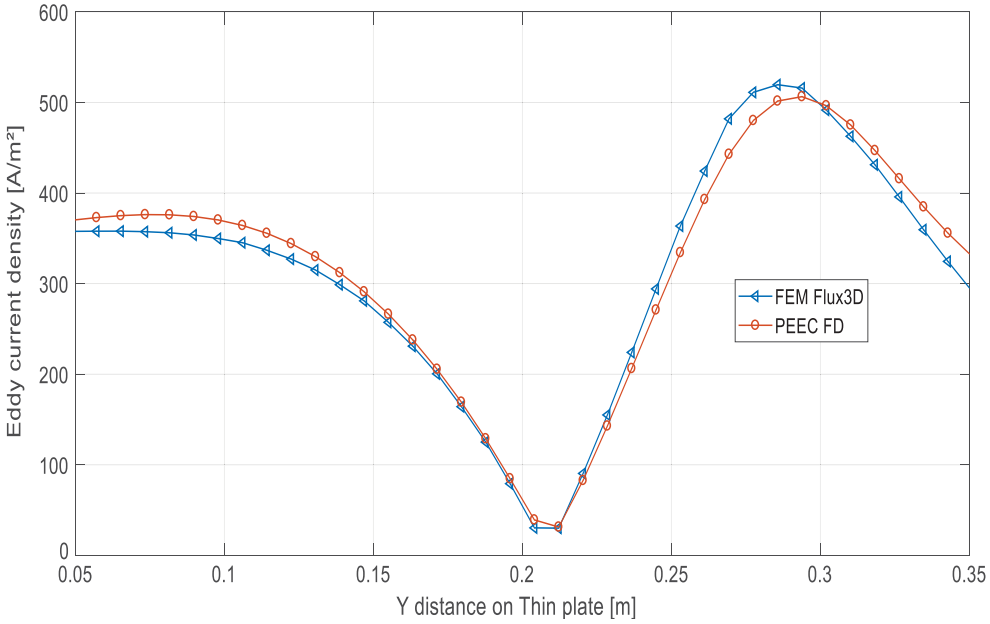


**Figure 10.** Eddy current comparison between FEM and PEEC/FD.

From these lasts, we can observe a good distribution of curves for the two approaches with slight differences due principally to several factors. We can cite the differences on meshes topologies (numbers of nodes and elements and their repartitions that cause the increase of iterations errors, the 3D elements in FEM against totally 2D in FDM), and the interactions are calculated analytically and then inserted in the global numerical systems for PEEC/FDM which offer more precision against the total numerical procedure implemented for FEM. Adding to this, the PEEC/FD is very fast compared to FEM method and can be implemented in many programming codes.

## 3. CONCLUSION

In the present work, we have proposed a new coupling procedure for calculating eddy currents in thin conductive and magnetic plates. In the first step, we have presented the appropriate electromagnetic model in which the currents circulate tangentially, and the magnetisation is considered by its perpendicular effect. The choice of the FDM is justified by the creation of rectangular surface elements. They are very suitable for analytically resolving the integrals in relation with the magnetization and eddy currents expressions. By analytical results, we can get more precision and robustness leading to a significant reduction in memory requirements and computation time. Another great advantage in this work is the detailed manner for calculating magnetic field from arbitrary oriented complex configuration coils, in which Euler transformations are mainly used for at least two considerable directions. This approach has the potential to affect numerous 3D electromagnetic applications using abundant programming languages, and it is also suitable for any optimization process. With the recent developments in nonhomogeneous FDM and their use for modern 2D materials and thin films, this approach can be an enormous asset in electrical characterization or simply in numerical modelling.

## ACKNOWLEDGMENT

Funding was provided by the General Direction of Research and Development Technologies/Ministry of Higher Education and Research Sciences DGRSDT/MERS (ALGERIA).

## REFERENCES

1. Dodd, C. V. and W. E. Deeds, "Analytical solutions to eddy-current probe-coil problems," *Journal of Applied Physics*, Vol. 39, No. 6, 2829–2838, 1968.
2. Bowler, J. R., "Eddy-current interaction with an ideal crack. 1: The forward problem," *Journal of Applied Physics*, Vol. 75, No. 12, 8128–8137, 1994.
3. Chebout, M., M. R. Mekideche, A. Hafaifa, A. Kouzou, and H. Allag, "Impedance measurement and computation for the steam generator tube integrity using the ECNDT technique," *Elektrotehniški Vestnik*, Vol. 85, No. 5, 235–240, 2018.
4. Maraspin, F. P., P. Bevilacqua, and P. Rem, "Modelling the throw of metals and nonmetals in eddy current separations," *International Journal of Mineral Processing*, Vol. 73, No. 1, 1–11, 2004.
5. Nagel, J. R., "Fast finite-difference calculation of Eddy currents in thin metal sheets," *Applied Computational Electromagnetic Society Journal*, Vol. 33, No. 6, 575–584, 2018.
6. Okress, E. C., D. M. Wroughton, G. Comenetz, P. H. Brace, and J. C. R. Kelly, "Electromagnetic levitation of solid and molten metals," *Journal of Applied Physics*, Vol. 23, No. 5, 545–552, 1952.
7. Fromm, E. and H. Jehn, "Electromagnetic forces and power absorption in levitation melting," *British Journal of Applied Physics*, Vol. 16, No. 5, 653–662, 1965.
8. Dholu, N., J. R. Nagel, D. Cohrs, and R. K. Rajamani, "Eddy current separation of nonferrous metals using a variable-frequency electromagnet," *KONA Powder and Particle Journal*, Vol. 34, 241–247, 2017.
9. Smith, Y. R., J. R. Nagel, and R. K. Rajamani, "Electrodynamic Eddy current separation of end of-life PV," *Energy Technology, The Minerals, Metals and Materials Series*, 379–386, Springer, Cham., 2017.

10. Ray, J. D., J. R. Nagel, D. Cohrs, and R. K. Rajamani, "Forces on particles in time-varying magnetic fields," *KONA Powder and Particle Journal*, Vol. 35, 251–257, 2018.
11. Fireteanu, V., B. Paya, J. Nuns, and T. Tudorache, "Electromagnetic levitation of solid and molten metals," *Journal of Applied Physics*, Vol. 21, No. 4, 581–590, 2002.
12. Yin, W., A. J. Peyton, and S. J. Dickinson, "Simultaneous measurement of distance and thickness of a thin metal plate with an electromagnetic sensor using a simplified model," *IEEE Transactions on Instrumentation and Measurement*, Vol. 53, No. 4, 1335–1338, 2004.
13. Betta, G., L. Ferrigno, M. Laracca, P. Burrascano, M. Ricci, and G. Silipigni, "An experimental comparison of multi-frequency and chirp excitations for eddy current testing on thin defects," *Measurement*, Vol. 63, 207–220, 2015.
14. Tian, L. L., C. Yin, Y. H. Cheng, and L. Bai, "Successive approximation method for the measurement of thickness using pulsed eddy current," *IEEE Instrumentation and Measurement Technology Conference*, 848–852, 2015.
15. N. Ida, Y. Le Menach, and T. Henneron, "High order surface impedance boundary conditions with the A-Φ formulation," *Facta Universitatis (NIS)*, Vol. 24, 147–155, 2011.
16. Zaidi, H., L. Santandréa, G. Krebs, and Y. Le Bihan, "Modelling of 3D thin regions in magnetostatic NDT using overlapping elements in dual formulations," *PIERS Proceedings*, 166–170, Marrakesh, Morocco, Mar. 20–23, 2011.
17. Ruehli, A., G. Antonini, and L. Jiang, *Circuit Oriented Electromagnetic Modelling Using the PEEC Techniques*, Wiley-Blackwell, 2017.
18. Ruehli, A. E., "Inductance calculation in a complex integrated circuit environment," *IBM Journal Research Development*, 470–480, 1972.
19. Hoer, C. and C. Love, "Exact inductance equations for rectangular conductors whith applications to more complicated geometries," *Journal of Research of the National Bureau of Standards-C. Engineering and Instrumentation*, Vol. 69, No. 2, 127–137, 1965.
20. Paul, C. R., *Inductance Loop and Partial*, John Wiley Sons, Inc., 2010.
21. Antonini, G., A. Orlandi, and C. R. Paul, "Internal impedance of conductors of rectangular cross section," *IEEE Transactions on Microwave Theory and Techniques*, Vol. 47, No. 7, 979–985, 1999.
22. Zhong, G. and C. K. Koh, "Exact closed-form formula for partial mutual inductances of rectangular conductors," *IEEE Transactions on Magnetics*, Vol. 50, No. 1, 1349–1352, 2003.
23. Wollenberg, C. and A. Gurisch, "Analysis of 3-D interconnect structures with PEEC using SPICE," *IEEE Trans. on Electromag. Compat.*, Vol. 41, No. 4, 412–417, 1999.
24. Cao, Y., Z. F. Li, J. F. Mao, and J. F. Mao, "A PEEC with a new capacitance model for circuit simulation of interconnects and packaging structures," *IEEE Trans. on Microwave Theory and Tech.*, Vol. 48, No. 9, 1435–1442, 2000.
25. Gope, D., A. Ruehli, and V. Jandhyala, "Solving low-frequency EM-CKT problems using the PEEC Method," *IEEE Trans. on Adv. Packaging*, Vol. 30, No. 2, 313–320, 2007.
26. Antonini, G., "PEEC capacitance extraction of 3-D interconnects," *IET Science, Measurement and Technology*, Vol. 1, No. 4, 201–209, 2007.
27. Le-Duc, T., O. Chadebec, J. M. Guichon, and G. Meunier, "Coupling between partial element equivalent circuit method and an integro-differential approach for solving electromagnetics problems," *IET Science, Measurement and Technology*, Vol. 6, No. 5, 394–397, 2012.
28. Kalimov, A., F. Kmos, B. Langenbeck, and G. Moritz, "Dynamic processes in laminated magnets: Simulation and comparison with experimental results," *IEEE Trans. Appl. Supercond.*, Vol. 12, No. 1, 98–10, 2002.
29. Salon, S. J., B. Mathewson, and S. Uda, "An intergro-differential approach to eddy currents in thin plates," *IEEE Transactions on Magnetics*, Vol. 19, No. 6, 2405–2408, 1983.
30. Tsuboi, H., M. Tanaka, and T. Misaki, "Eddy current and deflection analyses of a thin plate in time-changing magnetic field," *IEEE Transactions on Magnetics*, Vol. 26, No. 5, 1647–1649, 1990.

31. Demenko, A. and J. Sykulski, "On the equivalence of finite difference and edge element formulations in magnetic field analysis using vector potential," *COMPEL: The International Journal for Computation and Mathematics in Electrical and Electronic Engineering*, Vol. 33, No. 1–2, 47–55, 2014.
32. Huang, J., W. Liao, and Z. Li, "A multi-block finite difference method for seismic wave equation in auxiliary coordinate system with irregular fluid-solid interface," *Engineering Computations*, Vol. 35, No. 1, 334–362, 2018.
33. Chapwanya, M., R. Dozva, and G. Gift Muchatibaya, "A nonstandard finite difference technique for singular Lane-Emden type equations," *Engineering Computations*, Vol. 36, No. 5, 1566–1578, 2019.
34. Mawlood, M., S. Basri, W. Asrar, A. Omar, A. Mokhta, and M. Ahmad, "Solution of Navier-Stokes equations by fourth-order compact schemes and AUSM flux splitting," *International Journal of Numerical Methods for Heat and Fluid Flow*, Vol. 16, No. 1, 107–120, 2006.
35. Momeni, K., Y. Ji, Y. Wang, S. Paul, S. Neshani, D. E. Yilmaz, Y. K. Shin, D. Zhang, J.-W. Jiang, H. S. Park, S. Sinnott, A. van Duin, V. Crespi, and L.-Q. Chen, "Multiscale computational understanding and growth of 2D materials: A review," *NPJ Computational Materials*, Vol. 6, No. 22, 2020.
36. Aissaoui, M., H. Allag, and J. P. Yonnet, "Mutual inductance and interaction calculation between conductor or coil of rectangular cross section and parallelepiped permanent magnet," *IEEE Transactions on Magnetics*, Vol. 50, No. 11, 1–4, 2014.
37. Aomar, L., H. Allag, M. Feliachi, and J. P. Yonnet, "3-D integral approach for calculating mutual interactions between polygon-shaped massive coils," *IEEE Transactions on Magnetics*, Vol. 53, No. 11, 1–2, 2017.